Supporting Information

Cobalt/Zinc Dual-sites Coordinated with Nitrogen in Nanofibers Enabling Efficient and Durable Oxygen Reduction Reaction in Acidic Fuel Cells

Jian Zang,[ab]Feiteng Wang,[c] Qingqing Cheng,[ab]Xiao Liu,[ab]Lushan Ma,[ab]Chi Chen,[a]Lijun Yang,[d]Zhiqing Zou,[a]Daiqian Xie,*[c] and Hui Yang,*[a]

1.Experimental Section

1.1. Synthesis of Co/Zn-NCNF electrocatalyst

In a typical preparation, polyacrylonitrile (PAN, 1.6 g) was firstly dissolved in N,N-dimethyl formamide (DMF, 20 g), then heated to 70 °C and stirred for 1 hour until a uniform and transparent solution was formed. Subsequently, cobalt nitrate hexahydrate ($Co(NO_3)_2 \cdot 6H_2O$, 0.16 g), Pluronic F-127 (0.05 g) and nanosized zinc oxide (ZnO, 0.16 g, average size of ~30 nm) was added into the above-mentioned solution in turn before kept stirring for another 5 hours to form an emulsion. The obtained emulsion was then transferred into a plastic syringe (20 mL) to conduct to electrostatic spinning at 30 °C with a relative humidity of 45%. The syringe propulsion speed was 0.1 mm min^{-1} and the working distance between the collector and syringe end was ~15 cm. The operated voltage was kept at 18-20 kV. The obtained fibrous film was then put into the muffle furnace, heated to 240 ℃ for 2 hours with a ramp rate of 3 ℃ min^{-1}. The black fiber powder grinded was put in the porcelain boat to pyrolysis at 900 °C for 2 hours under N_2 atmosphere with a ramp rate of 5 °C min^{-1}, before the first etching under ammonia at 900 ℃ for 10 min. After immersed in 0.5 M H_2SO_4 solution under magnetic stirring for 6 hours at 80 ℃, the gained porous carbon fibers powder was washed with ultrapure water and dried under vacuum at 60 °C. Next, the product obtained was heated to 900℃ at a ramp rate of 5 ℃ min^{-1} in nitrogen atmosphere for the second pyrolysis, and then another ammonia etching was switched for 10 min to obtain the Co/Zn-NCNF nanofiber finally.

1.2. Characterization

Powder X-ray diffraction (XRD) patterns were tested on Bruker AXS D8 advance powder X-ray diffractometer with a Cu K_α (λ=1.5418 Å) radiation source, operating at 40 kV with 40 mA. Diffraction patterns were collected at a scanning rate of 2° min^{-1} and with a step size of 0.02°. TEM images were obtained by FEI Tecnai 30F microscope at an accelerating voltage of 200 kV. High angle annular dark field scanning transmission electron microscopy (HAADF-STEM) and X-ray energy dispersive spectrometry (EDS) mapping were performed on a double Cs-corrector FEI Titan Themis G2 60-300 microscope. X-ray photoelectron spectroscopy (XPS) was conducted using a Quantum 2000 Scanning ESCA Microprobe instrument with a monochromatic Al K_α source (1486.6 eV). The N1s spectra were deconvoluted by using a commercially available data fitting program (XPSPEAK41 software). The surface area was evaluated by the Brunauer-Emmett-Teller (BET) method on the instrument of ASAP-2020 using the adsorption branch in a relative pressure range from 0.01 to 1. The pore size distribution was derived from the adsorption branches of the isotherms using Barrett-Joyner-Halenda (BJH) model. Raman spectra were recorded on a Renishaw in Via Raman microscope with an Arion laser at the excitation wavelength of 514.5 nm. The X-ray absorption near-edge structure spectra were collected on BL14W1 beamline of Shanghai Synchrotron Radiation Facility (SSRF). Catalyst samples and reference compounds were measured in transmission mode for comparison and energy calibration. All XANES and EXAFS data were processed using Athena program.

1.3. Electrochemical measurements

Cyclic voltammetry (CV) and linear sweep voltammetry (LSV) were performed on rotating disk electrode (RDE, 5 mm diameter) which was polished by Al_2O_3 power, cleaned in ethanol solution/water and dried naturally. Then the 20 μl of the prepared catalysts slurry with concentration of 6 μg μl^{-1} was dropped on the glass carbon (GC) electrode to lead the catalyst loading of 0.6 mg cm^{-2}. As comparison, 4 μl Pt/C (20 wt.%) solution with concentration of 1

μg μl^{-1} was carefully dropped on the GC to get the catalyst loading of 20 μg_{Pt} cm^{-2}. Electrochemical tests were conducted on the CHI 730E equipped with a three-electrode system, using GC coated with as-prepared catalyst as working electrode, GC as counter electrode and Hg/Hg_2SO_4 as reference electrode. All the LSV tests were conducted in 0.1 M $HClO_4$ electrolyte with a rotation speed of 1600 rpm at a scan rate of 10 mV s^{-1}. Accelerated durability test (ADT) was conducted by cycling the catalyst with the potentials range from 0.6 to 1.1 V at a scan rate of 50 mV s^{-1} under continuous purging O_2 in electrolyte.

1.4. Electrochemical details

The Koutecky-Levich (K-L) plots were recorded by RDE measurement at various rotating speeds from 400 to 1600 rpm. The K-L equation is displayed as followed:

$$\frac{1}{j}=\frac{1}{j_L}+\frac{1}{j_K}=\frac{1}{B\omega^{1/2}}+\frac{1}{j_K}$$

$$B=0.2nFC_0D_0^{2/3}\nu^{-1/6}$$

where j is the measured current density, j_K and j_L are the kinetic and limiting current densities, ω is the revolutions per minute(rpm), n is the electron transfer number, F is the Faraday constant (96485 C mol^{-1}), C_0 is the bulk concentration of O_2 (1.2×10^{-6} mol cm^{-3}), D_0 is the diffusion coefficient of O_2 in electrolytes (1.9×10^{-5} cm^2 s^{-1}), and ν is the kinematic viscosity of the 0.1 M $HClO_4$ (0.0089 cm^2 s^{-1}).

Rotating ring disk electrode (RRDE, SD: 0.2475 cm^2) was measured to evaluate the hydrogen peroxide production (H_2O_2%) and electron transfer number (n) of ORR on samples.

$$H_2O_2\%=200\times\frac{\frac{I_r}{N}}{I_d+\frac{I_r}{N}}$$

$$n=4\times\frac{I_d}{I_d+\frac{I_r}{N}}$$

Where I_d is the disk current and I_r is the ring current, N=0.33 (calibrated) is the current collection efficiency of the Pt ring. The ring potential is fixed at 1.4 V/RHE.

1.5 Density functional theory (DFT)computational details

The spin-polarized first principle density-functional theory plus dispersion (DFT-D) calculations were carried out using the DMol^3 module in Materials Studio. The exchange-correlation functionals are based on generalized gradient approximation treated by the Perdew-Burke-Ernzerhof potential[1] with long range dispersion correction via Grimmer's scheme.[2] Core electrons were treated with DFT Semi-core pseudopotentials.[3] An all electron double numerical atomic orbital augmented by d-polarization function (DNP) was used as basis set. A smearing of 0.002 Hartree was applied to the orbital occupation. The self-consistent field (SCF) procedure was performed with a convergence threshold of 10^{-6} au on energy. Geometry optimizations were accomplished using the Broyden-Fletcher-Goldfarb-Shanno algorithm with a convergence threshold of 0.002 au/Å on the gradient, 0.005 Å on displacement, and 10^{-5} au on the energy. The real space global cutoff radius was set to be 5.0 Å. A conductor-like model (COSMO) was used to simulate a H_2O solvent environment with the dielectric constant setting as 78.54.[4] The zero-point energies and entropies of the ORR species were computed from the partial hessian vibrational analysis, in which only the adsorbates' vibrational modes were calculated explicitly. The energy barriers were obtained by linear synchronous transit/quadratic synchronous transit (LST/QST) methods in DMol^3 codes.The absolute electrode potential is related to its workfunction as follows, with the reversible hydrogen electrode (RHE) as the reference:

$$U = (\Phi - \Phi_{RHE})/e \quad \text{(S1)}$$

$$\Phi_{RHE} = (\Phi_{SHE} - 0.0592*pH) \quad \text{(S2)}$$

where Φ_{SHE} is the workfunction of the standard hydrogen electrode (we chose this value as 4.44eV).[5] The pH is set to 0 for the acidic electrolytes. It has to be noted that there would be some potential shifts along the reaction pathway due to the adsorption of different ORR

intermediates.[6] Goddard et al. demonstrated that the energy change caused by this potential shift is smaller than 0.01 eV, which is too small to be taken into consideration.[7] Therefore the following calculation would not consider such corrections.

References

[1] J. P. Perdew, K. Burke, M. Ernzerhof, *Phys Rev Lett* **1996**, 77, 3865.

[2] S. Grimme, *J Comput Chem* **2004**, 25, 1463.

[3] B. Delley, *Phys Rev B* **2002**, 66.

[4] A. Klamt, G. Schuurmann, *J Chem Soc Perk T 2* **1993**, DOI: 10.1039/p29930000799799.

[5] W. A. Donald, R. D. Leib, J. T. O'Brien, M. F. Bush, E. R. Williams, *J Am Chem Soc* **2008**, 130, 3371.

[6] a) K. Chant, J. K. Norskov, *J. Phys. Chem. Lett.* **2016**, 7, 1686; b) K. Chan, J. K. Norskov, *J. Phys. Chem. Lett.* **2015**, 6, 2663.

[7] T. Cheng, H. Xiao, W. A. Goddard, III, *J Am Chem Soc* **2016**, 138, 13802.

2. Supplementary Figures

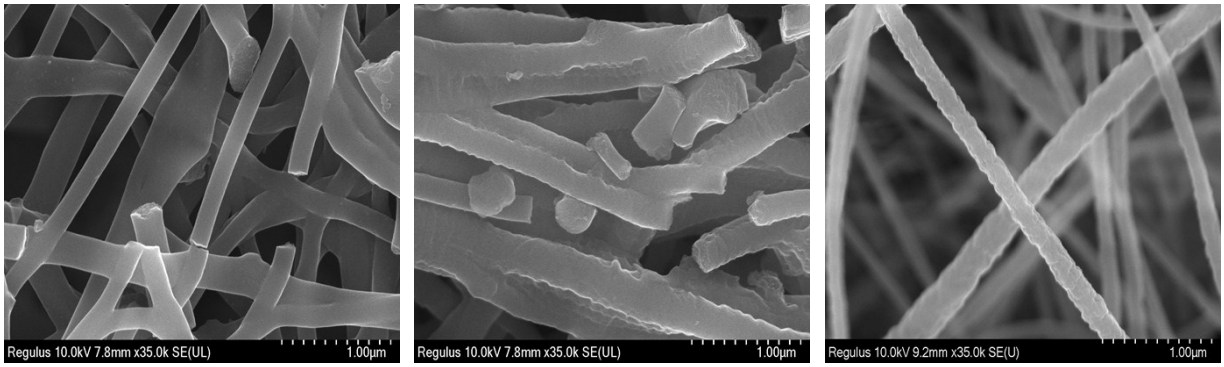

Fig. S1. SEM images of Co/Zn-NCNF

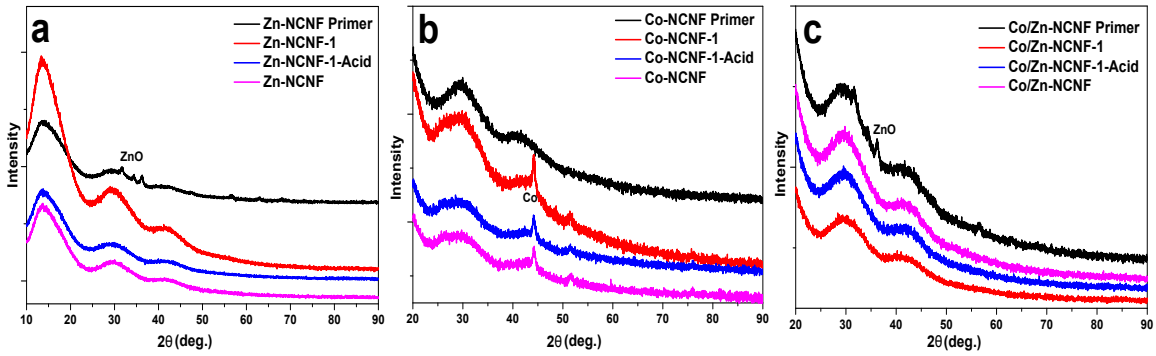

Fig. S2. XRD patterns of (a)Zn-NCNF, (b)Co-NCNF and (c)Co/Zn-NCNF in different steps of preparation.

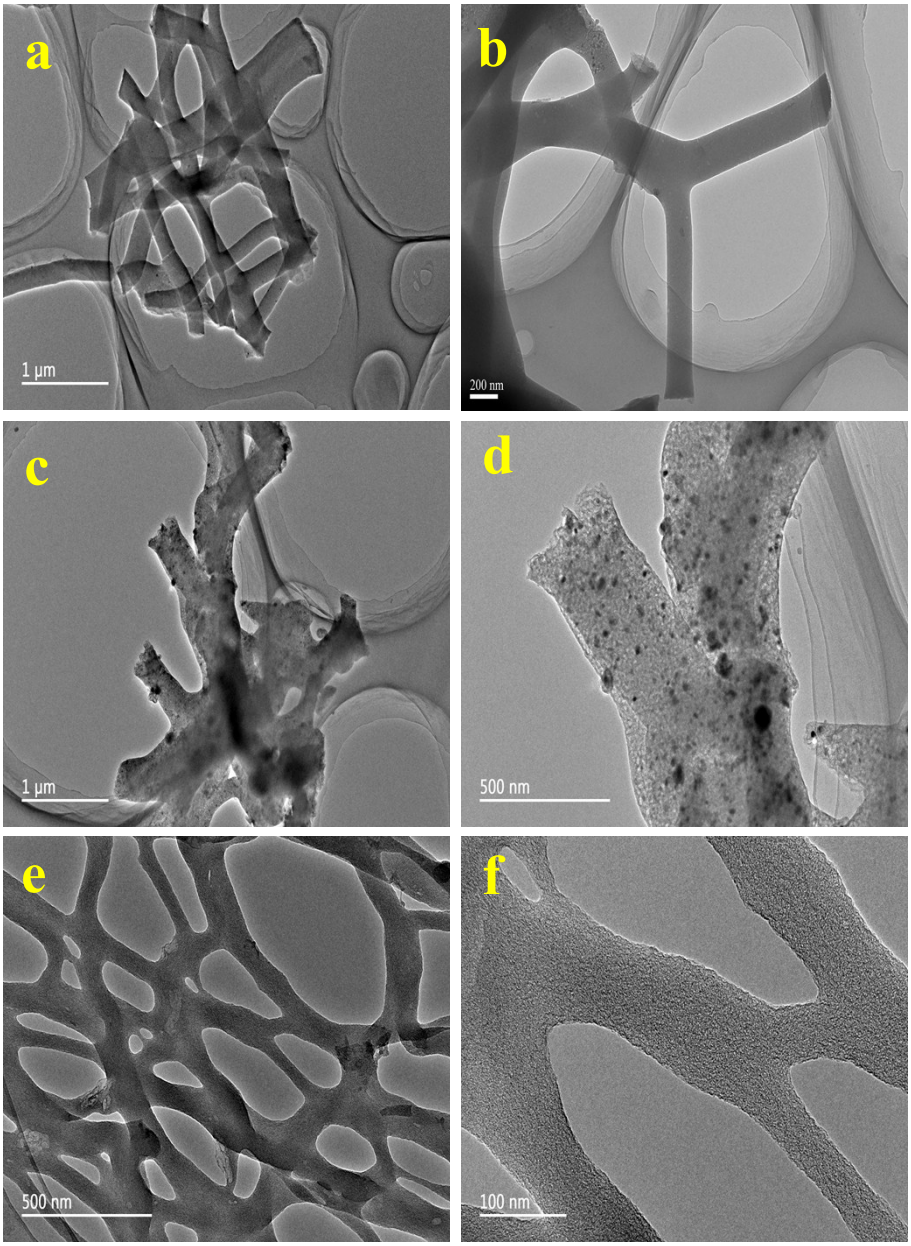

Fig. S3. TEM images of (a, b)Co/Zn-NCNF, (c, d) Co-NCNF, (e, f) Zn-NCNF.

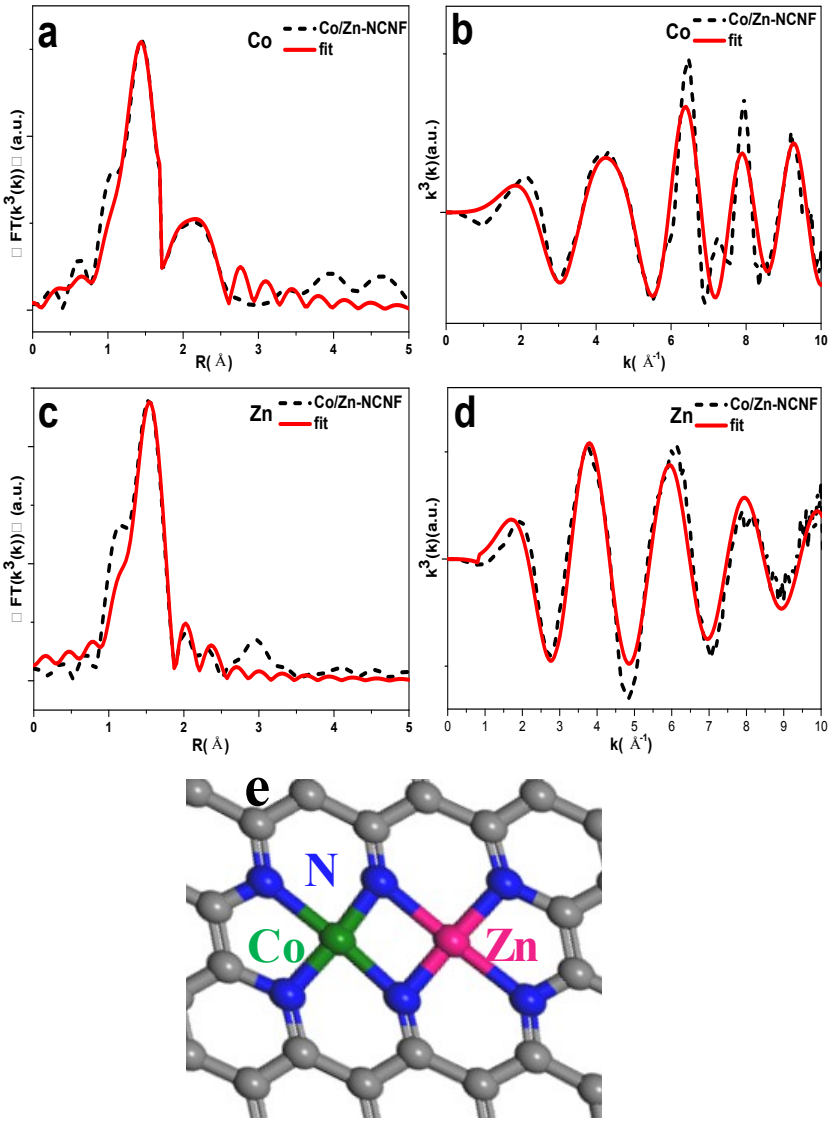

Fig. S4. (a) The Co K-edge Fourier-transform EXAFS of Co/Zn-NCNF and corresponding EXAFS fitting curves. (b) The corresponding EXAFS k space fitting curves of Co/Zn-NCNF. (c) The Zn K-edge Fourier-transform EXAFS of Co/Zn-NCNF and corresponding EXAFS fitting curves. (d) The corresponding EXAFS k space fitting curves of Co/Zn-NCNF. (e) Proposed architectures of Co/Zn dual sites.

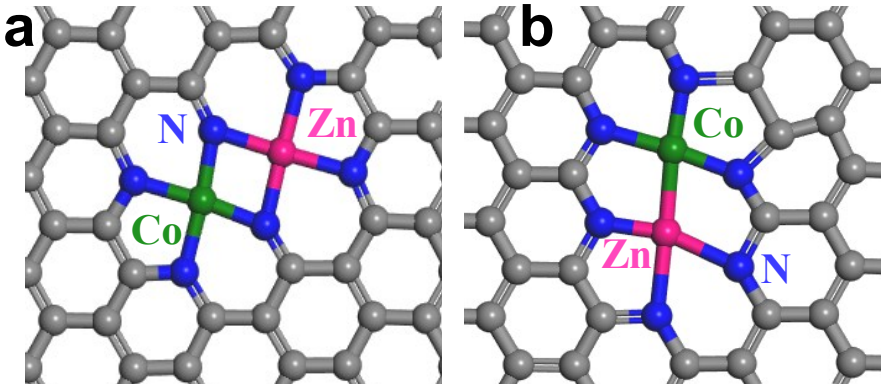

$N_2CoN_2ZnN_2$ (E_b: -11.2eV) N_3CoZnN_3 (E_b: -8.17eV)

Fig. S5. Optimized geometry of the $ZnCoN_6$ (a)$N_2CoN_2ZnN_2$, (b)N_3CoZnN_3 and corresponding binding energy (E_b).

The binding energy (E_b) is defined as $E_b = E_{M1M2N6C} - E_{M1} - E_{M2} - E_{N6C}$.

Where $E_{M1M2N6C}$ is the free energy of the dual-metal sites model, E_{M1} and E_{M2} are the energy of a single M metal in the vacuum, E_{N6C} is the free energy of the dual-metal model with the two metal centers removed.

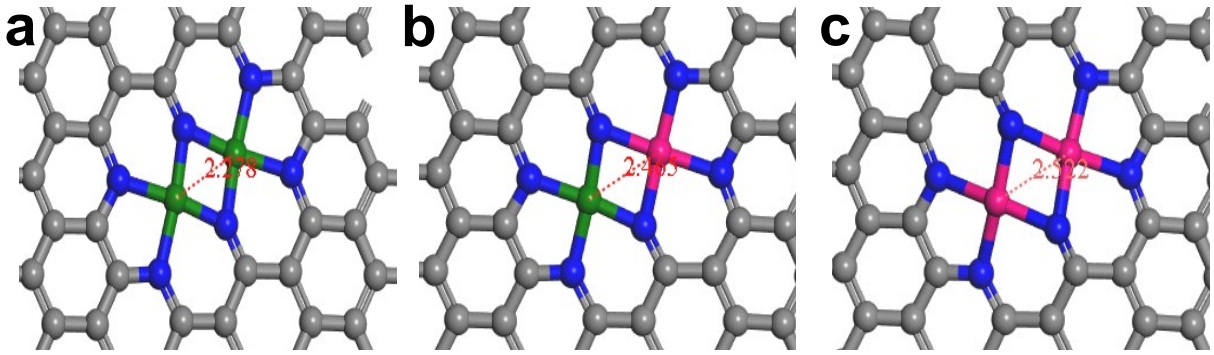

Fig. S6. Theoretical distances of metal atomic pairs of (a)$N_2CoN_2CoN_2$ (0.22nm), (b) $N_2CoN_2ZnN_2$ (0.24nm), (c)$N_2ZnN_2ZnN_2$(0.25nm)

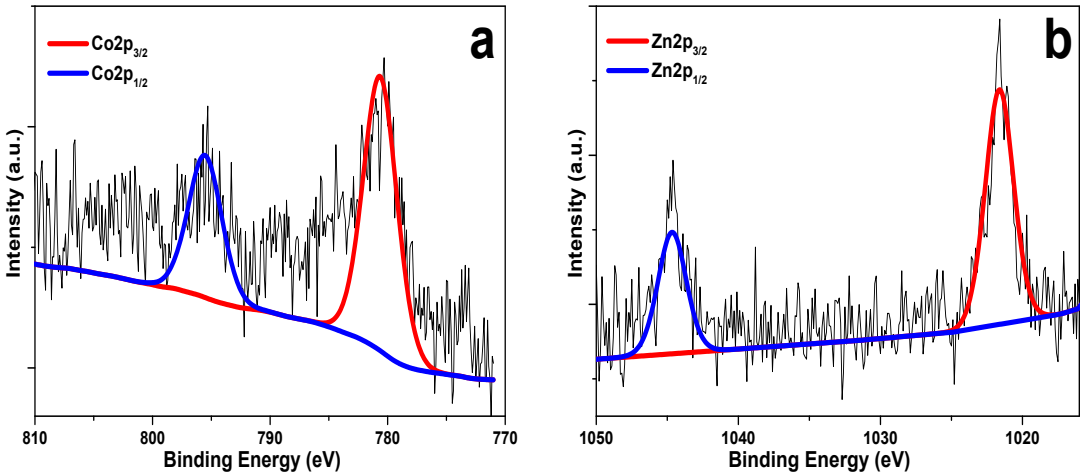

Fig. S7. XPS spectra of Co/Zn-NCNF. (a) Co 2p. and (b) Zn 2p.

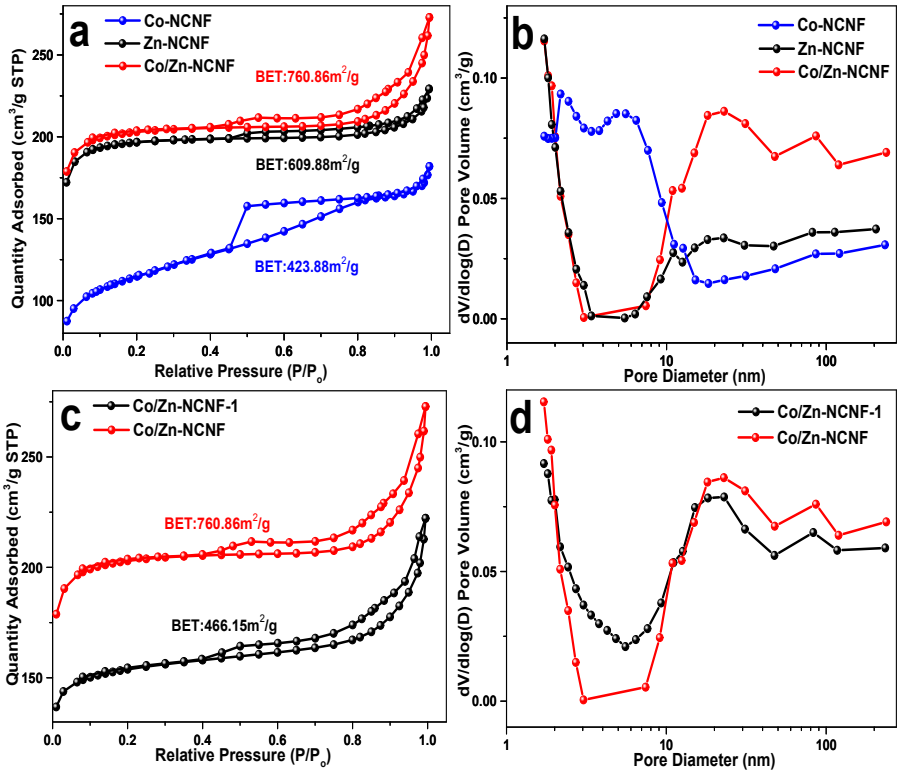

Fig. S8. (a) N_2 adsorption-desorption isotherms for Co-NCNF, Zn-NCNF and Co/Zn-NCNF, and (b) the corresponding pore-size distribution curves. (c) N_2 adsorption-desorption isotherms for Co/Zn-NCNF-1(the first NH_3-etching) and Co/Zn-NCNF, and (d) the corresponding pore-size distribution curves.

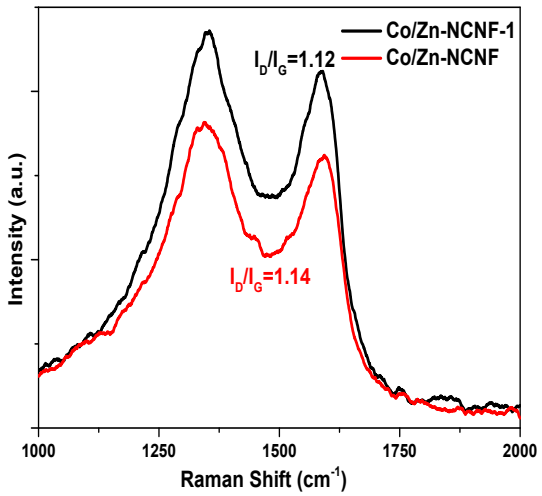

Fig. S9. Raman spectra of Co/Zn-NCNF. The intensity ratio of the D band (~1345 cm^{-1}) to G band (~1580 cm^{-1}) (I_D/I_G) for Co/Zn-NCNF in Raman spectra

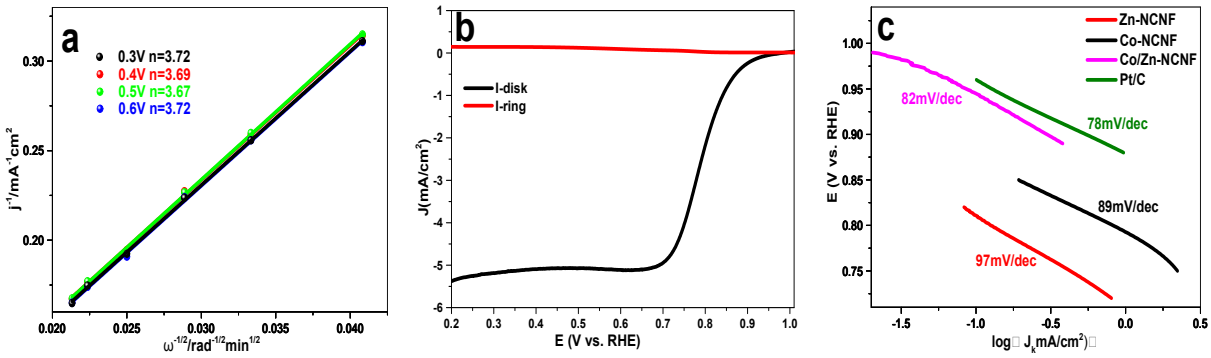

Fig. S10. (a) K-L plots at various potentials. (b) LSVs of rotating ring-disc electrode (RRDE). in 0.1 M $HClO_4$. Scan rate:10 mV s^{-1}. Rotating rate:1600 rpm. (c) Corresponding Tafel plots obtained from the RDE polarization curves.

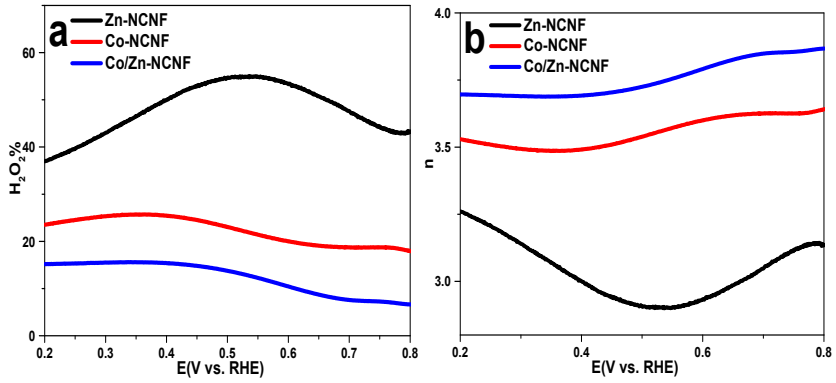

Fig. S11. (a) H_2O_2 yield and (b) electron transfer number for Zn-NCNF, Co-NCNF and Co/Zn-NCNF in 0.1 M $HClO_4$.

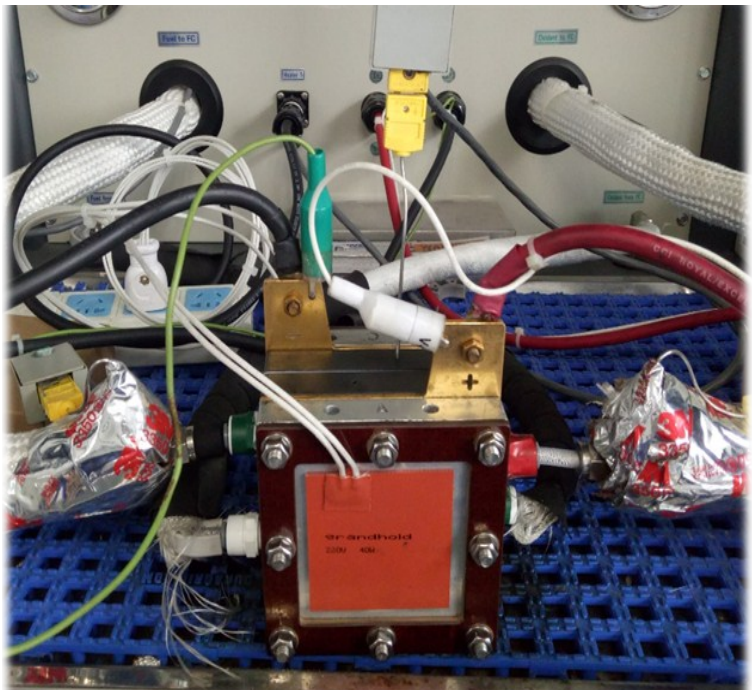

Fig. S12. Digital photographs of H_2-O_2 fuel cell

3. Supplementary Tables

Table S1. The fitting results of Co/Zn-NCNF.

Sample	Shell	N[a]	R_0(Å)[b]	σ^2(Å^2)[c]	ΔE_0(eV)[d]	R factor
Co	Co-N	2.9±0.5	1.89±0.02	0.005	8.2±2.2	0.01
	Co-M	1.0±0.1	2.49±0.01	0.003		
Zn	Zn-N	3.9±0.6	2.03±0.02	0.005	10.6±1.3	0.03
Remarks	S_0^2=0.72 is the amplitude reduction factor; [a]*N*: coordination numbers; [b]*R*: bond distance; [c]σ^2: Debye-Waller factors; [d] ΔE_0: the inner potential correction. *R* factor: goodness of fit.					

Table S2 Comparison of ORR activity of reported Co-based carbon catalysts in acid recently

Catalysts	Precursors	RDE activity ($E_{1/2}$, V vs RHE)	H_2–O_2 Fuel Cell performance		Ref.
			Maximum power density (W cm^{-2})	Durability test	
Co/Zn-NCNF	PAN,ZnO, $Co(NO_3)_2$	~0.8	0.603	~0.65V @0.4 A cm^{-2},150hours	This work
Co–N/CNFs	PAN, cobalt acetate, 4dimethylaminopyridine	0.7	/	/	1
Co–N–C nanofiber	DMF, PAN, $Co(NO_3)_2$	~0.4	/	/	2
Atomic Co–N–C	Co-doped ZIF-8	0.8	0.56	~0.2A cm^{-2} @0.7V, 100hours	3
Co/Zn$(mIm)_2$	Bimetal ZIF	0.76	0.374	~0.15 A cm^{-2} @0.5V, 100hours	4
Co–N–C-10	Co-doped ZIF-8	0.79	/	/	5
Co@SACo-N-C-10	PAN,$Co(Ac)_2$	0.778	0.42	~0.42V@0.3 A cm^{-2}, 100hours,(H_2-air)	6
LDH@ZIF-67-800	ZIF-67,CoAl-LDH	0.675	/	/	7
ZIF-TAA-p	ZIF-67, $Co(NO_3)_2$	0.78	/	/	8
Zn/CoN-C	Chitosan, $Co(Ac)_2$, $ZnCl_2$	0.796	0.705	~0.7V@0.5 A cm^{-2}, 8hours	9
Co-N-C@F127	ZIF-8,F127, $Co(NO_3)_2$	0.84	0.87	~0.2A cm^{-2} @0.7V, 100hours, (H_2-air)	10
HC-5Co95Zn	2-methylimidazole, $Co(NO_3)_2$, $Zn(NO_3)_2$	0.78	0.412	/	11
CNT-1	alkyne-modified CNTs, $Co(Ac)_2$, 5,15-bis-(pentafluorophenyl)-10-(4)-(1-azido)phenylcorrole,	0.78	/	/	12
Co-PPy-C	PPY, $Co(NO_3)_2$,	0.6	~0.2	~0.3A cm^{-2} @0.4V, 100hours, (H_2-air)	13
py-B12-M/C	B12,XC-72R	0.78	~0.26	~0.4A cm^{-2} @0.4V, 100hours, (H_2-air)	14
Co–N–C	Zn(II) zeolitic imidazolate framework, Co(II)Ac, 1,10-phenanthroline	0.7	0.3	/	15
$Co_3InC_{0.7}N_{0.3}$	Co-doped ZIF-8, $In(OH)_3$	~0.7	/	/	16

1. Q. Cheng, L. Yang, L. Zou, Z. Zou, C. Chen, Z. Hu and H. Yang, ACS Catalysis, **2017**, 7, 6864-6871.
2. X. Yan, K. Liu, T. Wang, Y. You, J. Liu, P. Wang, X. Pan, G. Wang, J. Luo and J. Zhu, Journal of Materials Chemistry A, **2017**, 5, 3336-3345.

3. X. X. Wang, D. A. Cullen, Y. T. Pan, S. Hwang, M. Wang, Z. Feng, J. Wang, M. H. Engelhard, H. Zhang, Y. He, Y. Shao, D. Su, K. L. More, J. S. Spendelow and G. Wu, Advanced materials, **2018**, 30, 1706758.

4. L. Chong, G. A. Goenaga, K. Williams, H. M. Barkholtz, L. R. Grabstanowicz, J. A. Brooksbank, A. B. Papandrew, R. Elzein, R. Schlaf, T. A. Zawodzinski, J. Zou, S. Ma and D.-J. Liu, ChemElectroChem, **2016**, 3, 1541-1545.

5. M. Xiao, H. Zhang, Y. Chen, J. Zhu, L. Gao, Z. Jin, J. Ge, Z. Jiang, S. Chen, C. Liu and W. Xing, Nano Energy, **2018**, 46, 396-403.

6. Q. Cheng, S. Han, K. Mao, C. Chen, L. Yang, Z. Zou, M. Gu, Z. Hu and H. Yang, Nano Energy, **2018**, 52, 485-493.

7. Z. Li, M. Shao, L. Zhou, R. Zhang, C. Zhang, M. Wei, D. G. Evans and X. Duan, Advanced materials, **2016**, 28, 2337-2344.

8. C. Zhang, B. An, L. Yang, B. Wu, W. Shi, Y.-C. Wang, L.-S. Long, C. Wang and W. Lin, Journal of Materials Chemistry A, **2016**, 4, 4457-4463.

9. Z. Lu, B. Wang, Y. Hu, W. Liu, Y. Zhao, R. Yang, Z. Li, J. Luo, B. Chi, Z. Jiang, M. Li, S. Mu, S. Liao, J. Zhang and X. Sun, Angewandte Chemie International Edition, **2019**, 131, 2648.

10. Y. H. He, S. Hwang, D. A. Cullen, M. A. Uddin, L. Langhorst, B. Y. Li, S. Karakalos, A. J. Kropf, E. C. Wegener, J. Sokolowski, M. J. Chen, D. Myers, D. Su, K. L. More, G. F. Wang, S. Litster and G. Wu, Energy & Environmental Science, **2019**, 12, 250-260.

11. Z. Meng, S. Cai, R. Wang, H. Tang, S. Song and P. Tsiakaras, Applied Catalysis B: Environmental, **2019**, 244, 120-127.

12. J. Meng, H. T. Lei, X. L. Li, J. Qi, W. Zhang and R. Cao, Acs Catalysis, **2019**, 9, 4551-4560.

13. H. T. Chung, G. Wu, Q. Li and P. Zelenay, International Journal of Hydrogen Energy,

2014, 39, 15887-15893.

14. C.-H. Wang, H.-C. Huang, S.-T. Chang, Y.-C. Lin and M.-F. Huang, RSC Adv., **2014**, 4, 4207-4211.

15. V. Goellner, V. Armel, A. Zitolo, E. Fonda and F. Jaouen, Journal of The Electrochemical Society, **2015**, 162, H403-H414.

16. H. Zhang, W. Xia, H. Shen, W. Guo, Z. Liang, K. Zhang, Y. Wu, B. Zhu and R. Zou, Angewandte Chemie, **2019**, DOI: 10.1002/anie.201911943.